HAL
open science

Axial Compressibility and Thermal Equation of State of Hcp Fe-5wt%Ni-5wt%Si

Eric Edmund, Francesca Miozzi, Guillaume Morard, Eglantine Boulard, Alisha Clark, Frédéric Decremps, Gaston Garbarino, Volodymyr Svitlyk, Mohamed Mezouar, Daniele Antonangeli

▶ **To cite this version:**

Eric Edmund, Francesca Miozzi, Guillaume Morard, Eglantine Boulard, Alisha Clark, et al.. Axial Compressibility and Thermal Equation of State of Hcp Fe-5wt%Ni-5wt%Si. Minerals, 2020, 10 (2), pp.98. ⟨10.3390/min10020098⟩. ⟨hal-02526718⟩

HAL Id: hal-02526718

https://hal.science/hal-02526718v1

Submitted on 31 Mar 2020

HAL is a multi-disciplinary open access archive for the deposit and dissemination of scientific research documents, whether they are published or not. The documents may come from teaching and research institutions in France or abroad, or from public or private research centers.

L'archive ouverte pluridisciplinaire **HAL**, est destinée au dépôt et à la diffusion de documents scientifiques de niveau recherche, publiés ou non, émanant des établissements d'enseignement et de recherche français ou étrangers, des laboratoires publics ou privés.

Autorisation HAL

HAL Authorization

minerals

MDPI

Article

Axial Compressibility and Thermal Equation of State of Hcp Fe–5wt%Ni–5wt%Si

Eric Edmund [1,2], Francesca Miozzi [1], Guillaume Morard [1,3], Eglantine Boulard [1], Alisha Clark [1,4], Frédéric Decremps [1], Gaston Garbarino [5], Volodymyr Svitlyk [5], Mohamed Mezouar [5] and Daniele Antonangeli [1,*]

[1] Sorbonne Université, Muséum National d'Histoire Naturelle, UMR CNRS 7590, Institut de Minéralogie, de Physique des Matériaux et de Cosmochimie, IMPMC, 75005 Paris, France; eric.edmund@hpstar.ac.cn (E.E.); francesca.miozzi@upmc.fr (F.M.); guillaume.morard@univ-grenoble-alpes.fr (G.M.); eglantine.boulard@upmc.fr (E.B.); alisha.clark@colorado.edu (A.C.); frederic.decremps@upmc.fr (F.D.)

[2] Centre for High Pressure Science & Technology Advanced Research (HPSTAR), Shanghai 201203, China

[3] Univ. Grenoble Alpes, Univ. Savoie Mont Blanc, CNRS, IRD, IFSTTAR, ISTerre, 38000 Grenoble, France

[4] Geological Sciences, University of Colorado, Boulder, CO 80309-0399, USA

[5] ESRF, F-38043 Grenoble, France; gaston.garbarino@esrf.fr (G.G.); svitlyk@esrf.fr (V.S.); mezouar@esrf.fr (M.M.)

* Correspondence: daniele.antonangeli@upmc.fr

Received: 4 December 2019; Accepted: 17 January 2020; Published: 23 January 2020

Abstract: Knowledge of the elastic properties and equations of state of iron and iron alloys are of fundamental interest in Earth and planetary sciences as they are the main constituents of telluric planetary cores. Here, we present results of X-ray diffraction measurements on a ternary Fe–Ni–Si alloy with 5 wt% Ni and 5 wt% Si, quasi-hydrostatically compressed at ambient temperature up to 56 GPa, and under simultaneous high pressure and high temperature conditions, up to 74 GPa and 1750 K. The established pressure dependence of the c/a axial ratio at ambient temperature and the pressure–volume–temperature (P–V–T) equation of state are compared with previous work and literature studies. Our results show that Ni addition does not affect the compressibility and axial compressibility of Fe–Si alloys at ambient temperature, but we suggest that ternary Fe–Ni–Si alloys might have a reduced thermal expansion in respect to pure Fe and binary Fe–Si alloys. In particular, once the thermal equations of state are considered together with velocity measurements, we conclude that elements other than Si and Ni have to be present in the Earth's inner core to account for both density and seismic velocities.

Keywords: iron alloys; nickel; silicon; high pressure; high temperature; equation of state; Earth's core; telluric planetary cores

1. Introduction

Different lines of evidence, from the analysis of meteorite compositions and Earth's differentiation models to the comparison of shock compression measurements with seismic observations, have put forward the notion that iron (Fe) is the main constituent of the Earth's core [1,2]. Cosmochemical arguments have also suggested that some weight percent (wt%) of nickel (Ni) is alloyed to iron [3], and, since Birch's pioneering work [1], it has been clear that elements lighter than an Fe–Ni alloy are present in the liquid outer core [2]. The density mismatch in the case of the solid inner core is less than that of the outer core, and though the fact that pure Fe is too dense in respect to seismic models

has been well-established, the accurate quantification of this density deficit is still an object of active research (e.g., [4,5]).

Concerning inner core density, the effect of Ni is generally considered minor. Indeed, based on results obtained at high pressure and ambient temperature, Ni alloying seems to marginally affect the compressibility curves [6–8] and compressional sound velocities [9–11] of pure Fe. Possible effects of Ni on the shear sound velocity have been suggested [12], but calculations have indicated that these too should become negligible at inner core conditions [13]. However, studies of the elasticity of Fe–Ni alloys at simultaneous high-pressure, high-temperature conditions are very limited [9,13]. Face-centered cubic (fcc) Fe–Ni alloys are known to exhibit an anomalously low (almost zero) thermal expansion over a wide temperature range (the Invar effect) [14,15]. Anomalous compressibility has also been observed for certain ranges of pressure as a consequence of a pressure-induced Invar effect [16]. The degree to which such effects extend to the more moderate Ni concentration expected for the Earth's core (about 5 wt% [17]), and in the hexagonal close-packed (hcp) structure, which is expected to be stable at inner core pressure and temperature conditions [18,19], remain to be addressed. Additionally, the comparative effect of nickel and light elements on the elasticity and equation of state of a ternary alloy needs further investigation, with only few experimental studies in literature that have been limited to ambient temperature [7,8,10,12]. In particular, amongst the light elements that have been proposed to enter into the inner core composition, silicon has recently received much attention [7,8,10,19–23], as both core differentiation models [24,25] and isotopic arguments [26] have supported its presence at a small level of wt%.

The c/a axial ratio is another material property of interest for the characterization of the Earth's inner core, as this relates to elastic anisotropy in materials with an hcp structure. Recently, starting from a survey of previous work, the effect of pressure, temperature, and composition on the axial ratio of iron and alloys in the Fe–Ni–Si system have been parameterized [27]. However, the determination of axial ratios in static compression experiments is highly sensitive to the pressurizing conditions of the sample (e.g., [4,6]). Due to the challenges inherent in the generation of high static pressures under quasi-hydrostatic conditions, data on iron alloys became available only recently [8,21,23]. It follows that the direct determination of the axial ratios of iron alloys is critical to validate and improve such models to more adequately reflect actual material properties at the conditions of planetary interiors.

We thus carried out X-ray diffraction (XRD) measurements on a ternary Fe–Ni–Si alloy at high pressure and under simultaneous high pressure and high temperature conditions. Data have been used to establish the pressure dependence of the c/a axial ratio and the pressure–volume–temperature (P–V–T) equation of state. A comparison of the obtained results with previous work indicates that Ni does not affect the compressibility and axial compressibility of Fe–Si alloys at ambient temperature, but we suggest that Ni-bearing Fe–Si alloys might have a reduced thermal expansion. Hence, the effects of nickel should be considered when modeling the Earth's inner core or, more generally, iron-rich planetary cores.

2. Materials and Methods

An Fe–Ni–Si alloy with 5 wt% Ni and 5 wt% Si, hereafter referred to as Fe–5Ni–5Si, was synthesized by an ultra-rapid quench method at the Institut de Chimie et des Matériaux de Paris-Est, Paris, France, starting from Fe (99.9%, GoodFellow), Ni (99.9%, GoodFellow), and Si (99.9%, GoodFellow), following a protocol detailed in [28]. Sample composition and homogeneity were studied with an electron microprobe (Camparis center, Sorbonne Université, Paris, France) and with scanning electron microscopy (Institut de Minéralogie, de Physique des Matériaux et de Cosmochimie, IMPMC, Paris, France) analysis. The homogeneity of the sample was confirmed below the 1 μm scale, and the measured composition was observed within 0.3 (Ni and Si) and 0.7 (Fe) wt% of the nominal values.

High pressure was generated by using Le Toullec-type membrane-driven diamond anvil cells (DAC) equipped with Re gaskets and beveled diamonds with a culet size of 150/300 μm. Samples were scraped from a large, thin ribbon, and specimen dimensions were chosen such that there was no bridging between the sample and the diamonds, nor was there contact between the gasket and the

sample. Selected samples were 5–7 μm thick for ambient temperature measurements and 1–3 μm thick for measurements at high temperature.

For room temperature measurements, the Fe–Ni–Si alloy was loaded alongside Pt as a pressure calibrant [29], with neon as a pressure transmitting medium so to ensure quasi-hydrostatic compression over the pressure range of interest.

For measurements at high temperature, the Fe–Ni–Si alloy was sandwiched between dry KCl disks that served as a pressure transmitting medium and to thermally and chemically insulate the sample from the diamonds. KCl was also used as the pressure calibrant by employing the thermal equation of state (EoS) reported in [30] and the temperature correction for KCl outlined in [31]. After loading the DAC, the assembly was left open to dry in a vacuum oven at 130 °C for several hours, after which the DAC was closed. This practice ensured that the moisture content was minimal within the sample chamber.

Angle-dispersive XRD measurements were performed at beamline ID27 at the European Synchrotron Radiation Facility (ESRF). The monochromatic radiation (λ = 0.3738 Å) was focused to approximately 3 × 3 μm^2, horizontal x vertical full-with-half-maximum (FWHM). Diffraction patterns were collected on a MarCCD camera, with collection times of 30–60 s. Samples were heated on both sides by two continuous Nd:YAG fiber lasers (TEM00), each one supplying up to 110 W. Hot spots were approximately 20 μm in diameter, much larger than the FWHM of the focused X-ray beam. Temperatures were measured on both sides before and after XRD data collection, as well as on one side during data collection, by the spectroradiometric method while using a Planck fit of the observed blackbody radiation from the center of the heating spot. While absolute errors in temperature can be estimated on the order of 150 K, the measured temperature was seen to vary by less than 30 K during pattern collection (averaged over 3–5 measurements per diffraction pattern).

Diffraction images were calibrated against a CeO_2 standard and then radially integrated by using the Dioptas image processing software [32]. The integrated diffraction pattern was then analyzed by use of Le Bail fits in the software Jana 2006 [33].

3. Results

3.1. X-Ray Diffraction at High Pressure and Ambient Temperature

X-ray diffraction patterns were collected at ambient temperature in the stability field of the hcp structure between 21 and 56 GPa. A typical two-dimensional diffraction image and the corresponding integrated diffraction pattern are shown in Figure 1. All observed peaks are indexed as either belonging to sample or to the Ne pressure transmitting medium. Pressure was assessed from the measured volume of the Pt calibrant (collected independently from that of the sample by translating the cell a few microns from the sample position, before and after sample measurement). Aside from an intrinsic 1%–2% error in absolute pressure due to the systematic effects of pressure calibration, the primary source of quantifiable error in pressure measurement was due to the pressure drift between the calibrant and sample measurements. Errors due to volume determination are very difficult to quantify, as the calibrant EoS is often the outcome of combined studies, and heavily parameterized with the use of results from diffraction as well as other techniques (e.g., ambient pressure ultrasonics). The Le Bail method of fitting power diffraction patterns while using the standard crystallography software typically leads to an underestimation of uncertainties when the sample background is large, as in the case of studies employing diamond anvil cells [34]. Differences between determined pressures before and after sample measurements were less than 1 GPa at all pressures, and errors in pressure were generally less than 2%. The observation of the near-hydrostatic peak ratios for the hcp Fe–5Ni–5Si sample and the minimal misfit of the Le Bail fit to both the sample and calibrant diffraction patterns indicated that the effects of deviatoric stress were negligible for the present dataset. Due to the weak intensity of the Ne reflections at the sample and calibrant measurement positions, as well as their overlap with strong sample and Pt reflections, the volume of Ne could not reliably be used to determine the magnitude of pressure gradients within the cell, which were expected to be small [35].

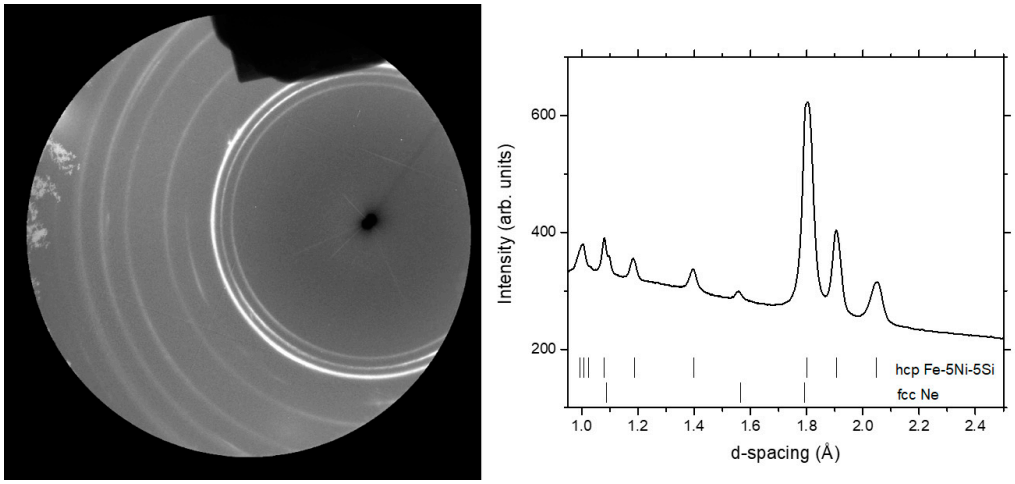

(**a**) (**b**)

Figure 1. Example of the collected data at high pressure and ambient temperature. (**a**) 2D diffraction image and (**b**) integrated diffraction pattern of Fe–5Ni–5Si at 55.7 GPa.

The obtained compression curve is reported in Figure 2 along with the literature results for pure Fe [4] and alloys in the Fe–Ni–Si system [8,21,23] that were compressed by using either He or Ne as a pressure transmitting medium. All data are generally consistent within mutual uncertainties, thus highlighting that the compressibility of iron at 300 K is not significantly modified over the here-considered pressure range by addition of either Ni or Si at a small wt% level. Accordingly, the presence of Ni and Si affect the density of an alloy essentially by slightly increasing it, when Ni is present, or decreasing it, when Si is present; according to their difference in atomic mass in respect to Fe.

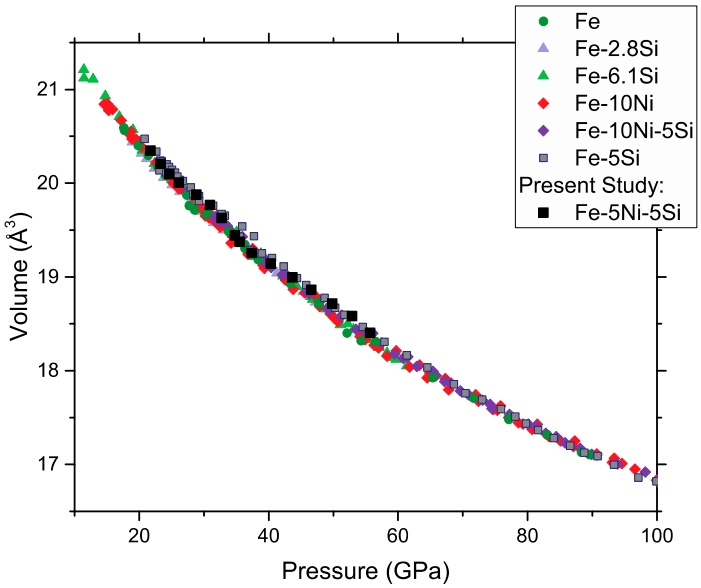

Figure 2. Isothermal compression curve of hexagonal close-packed (hcp) Fe–5Ni–5Si at ambient temperature compared to those of Fe [4] and Fe–Si alloys with 2.8 [21], 5 [23] and 6.1 wt% Si [21], an Fe–Ni alloy with 10 wt% Ni [8] and an Fe–Ni–Si alloy with 10 wt% Ni and 5 wt% Si [8], all in the hcp structure.

Conversely, as illustrated in Figure 3, both Si and Ni have a significant effect on the axial c/a ratio of the alloys, increasing it in respect to that of pure Fe while only moderately affecting its pressure dependence. As such, both Si and Ni are expected to qualitatively affect, in the same way, the elastic anisotropy of the alloy at ambient temperature. The pressure dependence of the c/a ratio of pure Fe and the effects on the c/a ratio when alloyed with 10 wt% Ni and when alloyed with 5 wt% Si were estimated by following the parameterization proposed in [27] (Figure 3). It stands clear that this model overestimates the c/a ratio of hcp Fe at low pressure, and it also overestimates its reduction with increasing pressure. On the other hand, the effect of Si and Ni inclusion are underestimated.

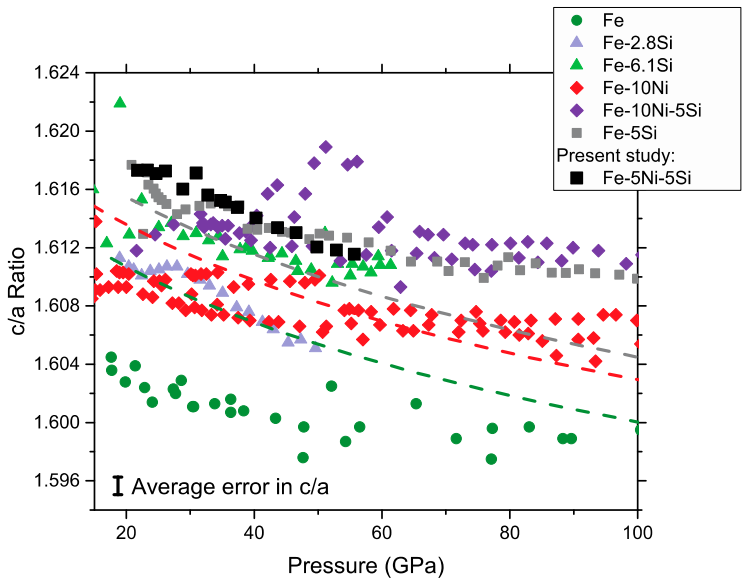

Figure 3. Axial c/a ratio of hcp alloys in the Fe–Ni–Si system at ambient temperature as a function of pressure. Legend is same as in that in Figure 2. Dashed lines are the expected c/a ratio according to the parameterization proposed in [27] for Fe (dark green), Fe–10Ni (red), and Fe–5Si (gray).

3.2. X-Ray Diffraction at High Pressure and High Temperature

X-ray diffraction patterns were collected under simultaneous high pressure and high temperature conditions along two isotherms, at 1450 K, upon compression up to about 74 GPa, and at 1750 K upon decompression. Temperatures varied by less than 50 K along each isotherm (1σ variation of 40 K for the 1450 K isotherm and 20 K for the 1750 K isotherm). A typical two-dimensional diffraction image and the corresponding integrated diffraction pattern are shown in Figure 4. All observed peaks are indexed either belong to the sample or to KCl. Pressure was increased (or decreased) step-wise by using a gas-driven membrane while the sample was maintained at high temperature via laser heating. The relative alignment of the focused X-ray spot, laser-heating system, and cell assembly was checked every 10–20 GPa. The application of high temperatures resulted in the relaxation of deviatoric stress in both the sample and the pressure-transmitting medium, becoming effectively negligible for high-temperature runs in the present study (quasi-hydrostatic conditions). This also ensured a comparable stress-state in both the compression and decompression runs. As previously mentioned in Section 3.1, standard crystallography softwares tend to underestimate error bars. Reported error bars for high temperature data were the determined by refitting the diffraction patterns with PDIndexer.

A single fcc phase was observed along the 1450 K isotherm up to 31–35 GPa, pressure above which this phase transformed into the hcp structure. Remnant traces of fcc diffraction lines were observed to 56 GPa. Along the 1750 K isotherm, an fcc phase was observed to crystallize upon decompression to pressures below 40 GPa. The entire pressure–volume–temperature (P–V–T) data

set measured for the hcp structure in this study, including data at ambient temperature, is reported in Figure 5.

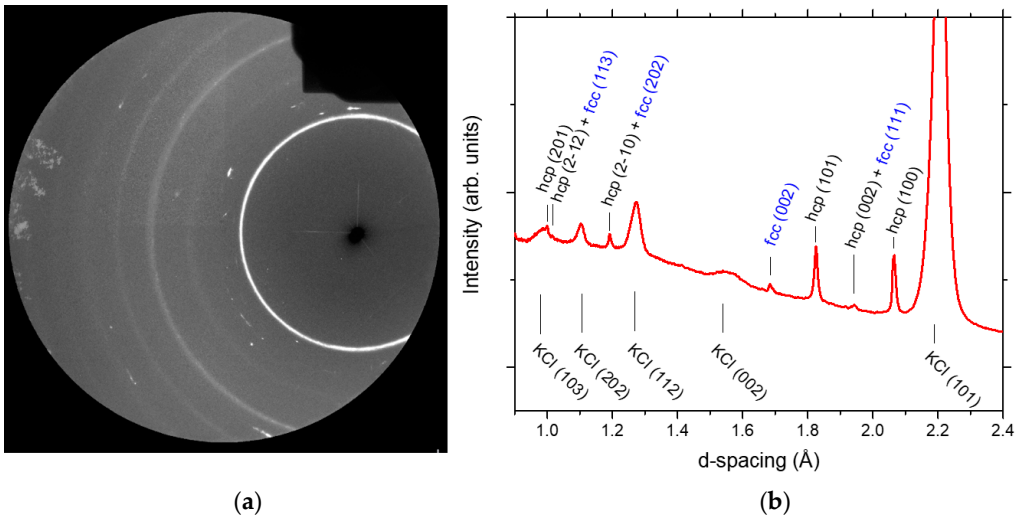

Figure 4. Example of the collected data at high pressure and high temperature. (**a**) 2D diffraction image and (**b**) integrated diffraction pattern of Fe–5Ni–5Si at 52 GPa and 1470 K.

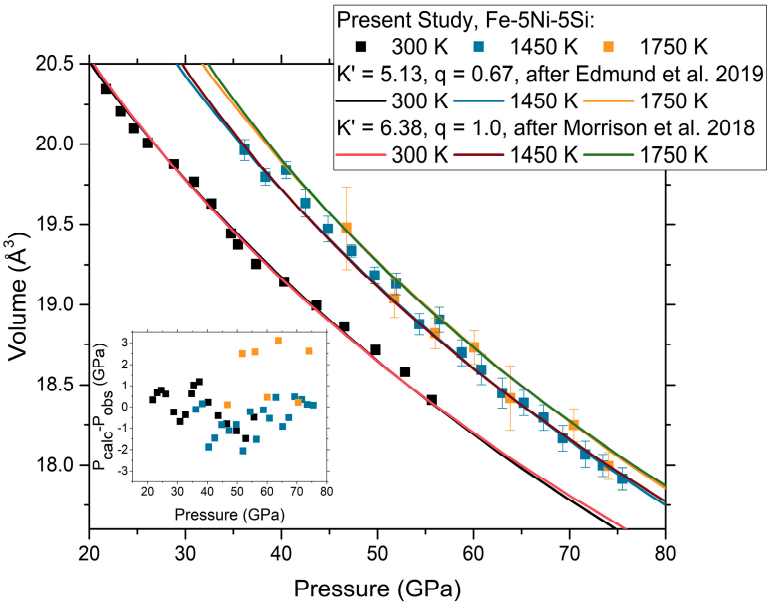

Figure 5. Isothermal compression curves of hcp Fe–5Ni–5Si at 300, 1450 and at 1750 K. Color-coded solid lines are the thermal equation of state fit to the experimental data, with the values of K′ and q fixed according to either Edmund et al., 2019 [23] or Morrison et al., 2018 [8]—cases 1 and 3, specifically. Inset: residuals in pressure for the present dataset (colors correspond to the respective isotherms of the main figure). See main text for more details.

Acquired data were used to establish a thermal equation of state (P–V–T EoS) following the formalism presented in [23]. Briefly, the ambient temperature component of the P–V–T thermal model was based on a Rydberg–Vinet equation of state

$$P_{300K}(\mathrm{V})=3K_0\left(\frac{1-\eta}{\eta^2}\right)\exp\left[\frac{3}{2}\,(K'-1)(1-\eta)\right] \quad (1)$$

where $\eta = \left(\frac{V}{V_0}\right)^{1/3}$, V is the unit cell volume, V_0 is the ambient pressure unit cell volume, K_0 is the bulk modulus, and K′ is its pressure derivative at ambient pressure and temperature. Minor differences in fitted elastic parameters can arise when using a different EoS formalism (e.g., Birch–Murnaghan vs. Rydberg–Vinet). The Rydberg–Vinet formalism was chosen here because it is generally accepted to better reflect the compressional behavior of metals at high pressures compared to other finite-strain equations of state [36,37].

The thermal pressure includes vibrational (P_{vib}) and electronic and anharmonic (P_{el+anh}) terms:

$$P(V,T) = P_{300K}(V) + P_{vib}(V,T)|_{300}^{T} + P_{el+anh}(V,T)|_{300}^{T} \quad (2)$$

The vibrational term of the thermal pressure can be written as:

$$P_{vib}(V,T) = \frac{9R\gamma_{vib}}{V}\left[\frac{\theta_D}{8} + T\left(\frac{T}{\theta_D}\right)^3 \int_{300}^{\theta_D/T} \frac{x^3}{\exp(x)-1}dx\right] \quad (3)$$

where γ_{vib} is the vibrational Grüneisen parameter, θ_D is the Debye temperature, and R is the ideal gas constant.

The volume dependence of the vibrational Grüneisen parameter and Debye temperature are, respectively, given by:

$$\frac{\gamma_{vib}}{\gamma_{vib,0}} = \left(\frac{V}{V_0}\right)^q \quad (4)$$

$$\theta_D = \theta_{D,0}\exp\left[\left(\gamma_{vib,0} - \gamma_{vib}\right)/q\right] \quad (5)$$

where q is an exponent that characterizes the volume dependence.

As both P_{el} and P_{anh} scale as T^2, a single term was used in the fitting procedure:

$$P_{el+anh}(V,T) = \frac{\gamma_e}{V}\beta_0\left(\frac{V}{V_0}\right)^k T^2 \quad (6)$$

where γ_e is the electronic Grüneisen parameter, β_0 is the electronic heat capacity, and k is an exponent that characterizes the volume dependence.

Though the variation from study to study across the literature in terms of data points at ambient temperature is small (see Figure 2), the reported values for V_0, K_0 and K′ vary up to about 3%, 40% and 35%, respectively [4,8,21,23]. As all these studies were performed employing Ne or He as a pressure transmitting medium and with pressure calibrations that are generally in close agreement (e.g., [38,39]), we argue that such discrepancies likely arise primarily from technical challenges that are associated with very high pressures generation and the strong covariance between V_0, K_0 and K′ [5,8]. In regards to the former, at Mbar pressures, it is expected that all pressure-transmitting media develop non-negligible stress gradients across the sample chamber [38,40] that may represent a systematic bias among these studies and strongly contribute to the differences between the available quasi-hydrostatic EoS for the Fe–Ni–Si system (e.g., [4,8,23]). In regard to the latter, the lack of direct measurements on the V_0 of hcp iron and iron alloys, these being high-pressure phases, directly reflects on the ambient temperature EoS parameters, which are particularly sensitive to the investigated pressure range, the employed pressure metrology, and the stress-state of both the sample and the calibrant. The fitting of only the 300 K data of the present study with a fixed K′ value systematically resulted in values of V_0 and K_0 that were in agreement with those reported in studies over a similar pressure range (e.g., [21]) but were higher in respect to studies that used the same value of K′ but covered a larger pressure range. The simultaneous refinement of both ambient and high temperature datasets provides a closer agreement with the V_0 and K_0 reported by studies that extended to higher pressures [8,23], likely due to the expanded pressure range of the high T data and the cancellation of experimental errors across the measured isotherms. Given the uncertainty in K′ for the Fe–Si alloys, q was kept fixed because it is related to the variation of K′ with temperature [41] and strongly dependent on the fixed value of K′ when left as a free parameter. In view of the overall limited pressure and temperature range covered in this

study and in order to better highlight the effects due to Ni, the values for K′, q and θ_D were either fixed to those established for Fe–5Si [23] (cases 1 and 2) or to those proposed for Fe–10Ni–5Si [8] (cases 3 and 4). Furthermore, given the considerable uncertainties over the role of anharmonic effects in the thermal EoS of iron and iron alloys, Table 1 includes fits to the present dataset with (cases 1 and 3) or without (cases 2 and 4) the incorporation of an anharmonic term. When an anharmonic term was incorporated, following previous studies, γ_e, β_0 and k were fixed to 2, 3.2 and 1.34, respectively [23]. In particular, value of β_0 was chosen in between previously reported values of 3.9 [5] and ~1.7 [4]—it must be noted, however, that the latter employed a different parameterization which led to small differences in pressure dependence, as it separately treated lattice and electronic anharmonicity. As highlighted in Figure 5, these fitting strategies similarly accounted for experimental data (as a matter of fact, the fits are virtually indistinguishable over the investigated pressure and temperature range).

Table 1. Pressure–volume–temperature equation of state (P–V–T EoS) fitting parameters for hcp Fe–5Ni–5Si (cases 1–4) and reported thermoelastic parameters for Fe–5Si [23] and Fe–10Ni–5Si [8]. For cases 1–4, when errors are not given, the parameter was kept fixed (see main text).

Case#	V_0 (Å^3)	K_0 (GPa)	K′	θ_D (K)	$\gamma_{vib,0}$	q	γ_e	β_0(10^{-6}·cm^3·mol^{-1}·J·K^{-1})	k
1	22.61 ± 0.08	160 ± 5	5.13	422 [1]	1.66 ± 0.09	0.67	2	3.2	1.34
2	22.61 ± 0.07	160 ± 5	5.13	422 [1]	2.13 ± 0.08	0.67	-	-	-
3	22.97 ± 0.10	125 ± 5	6.38	417 [1]	1.82 ± 0.09	1	2	3.2	1.34
4	22.97 ± 0.09	125 ± 4	6.38	417 [1]	2.30 ± 0.09	1	-	-	-
[23]	22.59	163	5.13	422	1.73	0.67	2	3.2	1.34
[8]	22.84	125	6.38	417	2	1	†	†	†

[1] Literature values for θ_D in hcp Fe and Fe–Si alloys ranged between 417 and 422 K [5,8,23,42,43]. Actual values within this range do not affect fit quality or other fitting parameters.† Reference [8] employed anharmonic thermal pressure corrections after reference [4].

When the P–V–T EoS determined here for hcp Fe–5Ni–5Si is compared to the P–V–T EoS of hcp Fe–5Si [23] (Figure 6), the effects of the inclusion of 5 wt% Ni are found to be very minor on compressibility (P–V curves of Fe–5Ni–5Si and Fe–5Si are almost parallel along the three isotherms), while the Ni-bearing Fe–Si alloys appear to have a somewhat reduced thermal expansion. Indeed, the volumes of Fe–5Ni–5Si along the high temperature isotherms are systematically below those of Fe–5Si (although the difference is small). All data presented in this study may be found in the Supplementary Information.

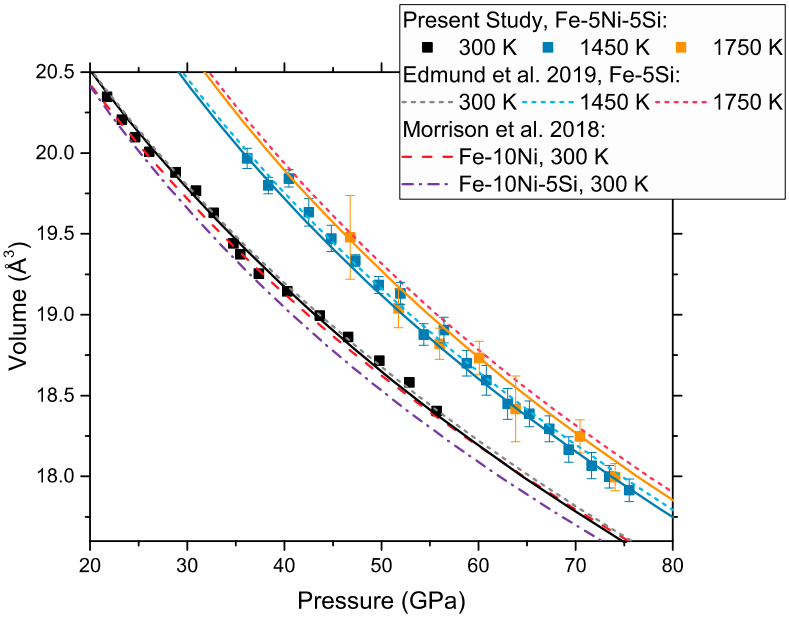

Figure 6. Comparison of the isothermal compression curves of hcp Fe–5Ni–5Si at 300, 1450 and 1750 K with literature results on Fe–Si, Fe–Ni and Fe–Ni–Si alloys. Color-coded solid lines are the thermal equation of state fit to the experimental data (see Figure 5 and discussion in the main text). P–V–T relations for hcp Fe–5Si [23] are also reported as dotted curves (same temperature–color code). Dashed and dash-dotted lines are the P–V relation established at 300 K for hcp Fe–10Ni and hcp Fe–10Ni–5Si, respectively [8]. While compression curves at ambient temperature do not show differences, the high-temperature compression curves of Fe–5Ni–5Si are parallel but systematically below those of Fe–5Si, suggesting a reduced thermal expansion.

4. Discussion

Seismic studies have argued for an elastically anisotropic inner core [44–46], and this feature has been commonly ascribed to the preferential alignment of comprising crystals (e.g., [47,48]). The elastic anisotropy of the hcp-structured materials in the meridian a–c plane is largely governed by the ratio of the elastic moduli C_{33}/C_{11} which, in turn, can be related to the axial compressibility and, hence, to the c/a axial ratio. In agreement with previous measurements [8], both nickel and silicon are individually observed to increase the c/a axial ratio in binary Fe–Si and Fe–Ni alloys in respect of pure iron, while the effect on its pressure dependence is less evident (Figure 3). Interestingly, we note that Ni addition does not significantly modify the c/a ratio of the Fe–Si alloys. As illustrated in Figure 3, Fe–5Ni–5Si and Fe–10Ni–5Si have the same c/a ratio as Fe–5Si. As already pointed out, the recently proposed parameterization of the effects of pressure, temperature and composition on the c/a axial ratio of the hcp Fe–Ni–Si alloys [27] fails to reproduce the values measured in quasi-hydrostatically compressed Fe, binary Fe–Si and Fe–Ni alloys, and ternary Fe–Ni–Si alloys.

To quantitatively correlate the c/a ratio with C_{33}/C_{11} and elastic anisotropy is not a straightforward exercise (see, for instance, discussion in [8]). Calculations pointed out the importance of the c/a ratio to derive the correct elastic moduli from stress–strain methods [49,50]. As the c/a ratio in Fe–Ni, Fe–Si and Fe–Ni–Si alloys is closer to the ideal value for hcp structure of 1.633 (Figure 3), we might expect the elastic anisotropy to be reduced in respect to pure Fe, but direct measurements remain necessary to substantiate this speculation.

Concerning inner core density, the current results do not allow for a reliable extrapolation to inner core conditions. Further measurements over an extended pressure and temperature range are planned. Nonetheless, a few considerations can be made. The negligible effect of nickel and silicon at a small wt% level on the compressibility of pure iron argues for substitutional alloys where Ni and/or Si randomly replace Fe in the crystal lattice without significantly modifying it. Thus, the main effect on density (and the only effect at ambient temperature) is the scaling according to relative atomic masses. On the other hand, thermal expansion seems to be smaller in hcp Fe–Ni–Si alloys than in pure hcp-Fe [5] and hcp-Fe–Si alloys [23]. On a qualitative ground, this is not surprising because fcc Fe–Ni alloys are known for their anomalously low thermal expansion. In hcp alloys and for moderate Ni concentration in the range expected for the Earth's core, such effect is much reduced but appears to still be present. Accordingly, nickel acts to increase the density of the alloy at inner core conditions by both the increased atomic mass of Ni in respect to Fe and because Ni-bearing alloys have comparatively smaller volume at core temperatures due to the reduced thermal expansion.

Based on these arguments, the effects of nickel vs. silicon alloying are qualitatively different in many aspects. Though both Ni and Si do not change the compressibility of Fe (Figures 2 and Figure 6), Ni increases density without significantly affecting compressional sound velocity [9–11,13], while Si decreases density and increases compressional sound velocity [10,20,23]. No composition within the binary Fe–Ni or Fe–Si system is expected to match both seismically observed velocities and densities at inner core conditions [13,20,23]. In particular, an Fe–Si alloy with 5 wt% Si can match the density of the Earth's inner core for all reasonable core temperatures, but its velocities remain too high in respect to seismological observations [23]. The addition of Ni would call for more Si to account for the inner core density, pushing the velocity of this ternary Fe–Ni–Si alloy even further away. Fe–Si alloys whose velocities are expected to get close to seismological observations are too

dense at relevant pressure and temperatures [20,23]. The addition of Ni would make the ternary Fe–Ni–Si alloy even denser. We can then conclude that no Fe–Ni–Si alloy can account for the seismically observed physical properties of the inner core and that elements other than Si and Ni have to be present in the Earth's inner core.

Supplementary Materials: The following are available online at www.mdpi.com/xxx/s1.

Author Contributions: Conceptualization, G.M. and D.A.; formal analysis, E.E. and F.M.; funding acquisition, F.D. and D.A.; investigation, E.E., F.M., G.M., E.B., A.C., G.G., V.S., M.M. and D.A.; project administration, D.A.; supervision, G.M., F.D. and D.A.; writing—original draft, E.E. and D.A.; writing—review and editing, F.M., G.M., E.B. and V.S. All authors have read and agreed to the published version of the manuscript.

Funding: This work was supported by the Investissements d'Avenir programme (reference ANR-11-IDEX-0004-02) and more specifically within the framework of the Cluster of Excellence MATriaux Interfaces Surfaces Environnement (MATISSE) led by Sorbonne Université. This project has received funding from the European Research Council (ERC) under the European Union's Horizon 2020 research and innovation programme (Grant agreement No. 724690). F.M. has received funding from the European Research Council (ERC) under the European Union's Horizon 2020 research and innovation Programme (Grant agreement 670787).

Acknowledgments: The authors wish to thank Jeroen Jacobs for technical assistance at the ESRF. Yoann Guarnelli and Paraskevas Parisiadis are acknowledged for their support at IMPMC. Femtosecond laser micro-machining at the Institut de Minéralogie, de Physique des Matériaux et de Cosmochimie (IMPMC), Paris, has been developed and realized by the "Cellule Projet" with the financial support of ANR 2010-JCJC-604-01.

Conflicts of Interest: The authors declare no conflict of interest. The funders had no role in the design of the study; in the collection, analyses, or interpretation of data; in the writing of the manuscript, or in the decision to publish the results.

References

1. Birch, F. Elasticity and constitution of the Earth's interior. *J. Geophys. Res.* **1952**, *57*, 227–286.
2. Poirier, J.P. Light elements in the Earth's outer core: A critical review. *Phys. Earth Planet. Inter.* **1994**, *85*, 319–337.
3. Li, J.; Fei, Y. Experimental constraints on core composition. In *Treatise on Geochemistry*; Elsevier: New York, NY, USA, 2007; pp. 1–31.
4. Dewaele, A.; Loubeyre, P.; Occelli, F.; Mezouar, M.; Dorogokupets, P.I.; Torrent, M. Quasihydrostatic equation of state of iron above 2 Mbar. *Phys. Rev. Lett.* **2006**, *97*, 215504.
5. Fei, Y.; Murphy, C.; Shibazaki, Y.; Shahar, A.; Huang, H. Thermal equation of state of hcp-iron: Constraint on the density deficit of the Earth's solid inner core. *Geophys. Res. Lett.* **2016**, *43*, 6837–6843.
6. Mao, H.K.; Wu, Y.; Chen, L.C.; Shu, J.F. Static compression of iron to 300 GPa and $Fe_{0.8}Ni_{0.2}$ alloy to 260 GPa: Implications for composition of the core. *J. Geophys. Res.* **1990**, *95*, 21737–21742.
7. Asanuma, H.; Ohtani, E.; Sakai, T.; Terasaki, H.; Kamada, S.; Hirao, N.; Ohishi, Y. Static compression of $Fe_{0.83}Ni_{0.09}Si_{0.08}$ alloy to 374 GPa and $Fe_{0.93}Si_{0.07}$ alloy to 252 GPa: Implications for the Earth's inner core. *Earth Planet. Sci. Lett.* **2011**, *310*, 113–118.
8. Morrison, R.A.; Jackson, J.M.; Sturhahn, W.; Zhang, D.; Greenberg, E. Equation of state and anisotropy of Fe-Ni-Si alloys. *J. Geophys. Res. Solid Earth* **2018**, *123*, 4647–4675.
9. Kantor, A.P.; Kantor, I.Y.; Kurnosov, A.V.; Kuznetsov, A.Y.; Dubrovinskaia, N.A.; Krisch, M.; Bossak, A.A.; Dimitriev, V.P.; Urusov, V.S.; Dubrovinsky, L.S. Sound wave velocities of fcc Fe-Ni alloy at high pressure and temperature by mean of inelastic X-ray scattering. *Phys. Earth Planet. Inter.* **2007**, *164*, 83–89.
10. Antonangeli, D.; Siebert, J.; Badro, J.; Farber, D.L.; Fiquet, G.; Morard, G.; Ryerson, F.J. Composition of the Earth's inner core from high-pressure velocity measurements in Fe-Ni-Si alloys. *Earth Planet. Sci. Lett.* **2010**, *295*, 292–296.
11. Wakamatsu, T.; Ohta, K.; Yagi, T.; Hirose, K.; Ohishi, Y. Measurements of sound velocity in iron-nickel alloys by femtosecond laser pulses in a diamond anvil cell. *Phys. Chem. Miner.* **2018**, *45*, 589–595.
12. Morrison, R.A.; Jackson, J.M.; Sturhahn, W.; Zhao, J.; Toellner, T.S. High pressure thermoelasticity and sound velocities of Fe-Ni-Si alloys. *Phys. Earth Planet. Inter.* **2019**, *294*, 106268.

13. Martorell, B.; Brodholt, J.; Wood, I.G.; Vočadlo, L. The effect of nickel on the properties of iron at the conditions of Earth's inner core: Ab initio calculations of seismic wave velocities of Fe-Ni alloys. *Earth Planet. Sci. Lett.* **2013**, *365*, 143–151.
14. Guillaume, C.E. Recherches sur les aciers au nickel. Dilatations aux temperatures elevees; resistance electrique. *CR Acad. Sci.* **1897**, *125*, 18.
15. Van Schilfgaarde, M.; Abrikosov, I.A.; Johansson, B. Origin of the Invar effect in iron-nickel alloys. *Nature* **1999**, *400*, 46–49.
16. Dubrovinsky, L.; Dubrovinskaia, N.; Abrikosov, I.A.; Vennström, M.; Westman, F.; Carlson, S.; van Schilfgaarde, M.; Johansson, B. Pressure-induced invar effect in Fe-Ni alloys. *Phys. Rev. Lett.* **2001**, *86*, 4851–4854.
17. McDonough, W.F.; Sun, S.S. Composition of the Earth. *Chem. Geol.* **1995**, *120*, 223–253.
18. Tateno, S.; Hirose, K.; Komabayashi, T.; Ozawa, H.; Ohishi, Y. The structure of Fe-Ni alloy in Earth's inner core. *Geophys. Res. Lett.* **2012**, *39*, L12305.
19. Tateno, S.; Kuwayama, Y.; Hirose, K.; Ohishi, Y. The structure of Fe-Si alloy in Earth's inner core. *Earth Planet. Sci. Lett.* **2015**, *418*, 11–19.
20. Antonangeli, D.; Morard, G.; Paolasini, L.; Garbarino, G.; Murphy, C.A.; Edmund, E.; Decremps, F.; Fiquet, G.; Bosak, A.; Mezouar, M.; et al. Sound velocities and density measurements of solid hcp-Fe and hcp-Fe-Si(9wt.%) alloy at high pressure: Constraints on the Si abundance in the Earth's inner core. *Earth Planet. Sci. Lett.* **2018**, *482*, 446–453.
21. Kamada, S.; Suzuki, N.; Maeda, F.; Hirao, N.; Hamada, N.; Hamada, M.; Ohtani, E.; Masuda, R.; Mitsui, T.; Ohishi, Y.; Nakano, S. Electronic properties and compressional behavior of Fe-Si alloys at high pressure. *Am. Mineral.* **2018**, *103*, 1959–1965.
22. Komabayashi, T.; Pesce, G.; Morard, G.; Antonangeli, D.; Sinmyo, R.; Mezouar, M. Phase transition boundary between fcc and hcp structures in Fe-Si alloys and its implications for terrestrial planetary cores. *Am. Mineral.* **2019**, *104*, 94–99**.**
23. Edmund, E.; Antonangeli, D.; Decremps, F.; Miozzi, F.; Morard, G.; Boulard, E.; Clark, A.N.; Ayrinhac, S.; Gauthier, M.; Morand, M.; et al. Velocity-density systematics of Fe-5wt%Si: Constraints on Si content in the Earth's inner core. *J. Geophys. Res. Solid Earth* **2019**, *124*, 3436–3447.
24. Siebert, J.; Badro, J.; Antonangeli, D.; Ryerson, F.J. Terrestrial accretion under oxidizing conditions. *Science* **2013**, *339*, 1194–1197.
25. Fischer, R.A.; Nakajima, Y.; Campbell, A.J.; Frost, D.J.; Harries, D.; Langenhorst, F. High pressure metal-silicate partitioning of Ni, Co, V, Cr, Si and O. *Geochim. Cosmochim. Acta* **2015**, *167*, 177–194.
26. Fitoussi, C.; Bourdon, B.; Kleine, T.; Oberli, F.; Reynolds, B.C. Si isotope systematics of meteorites and terrestrial peridotites: Implications for Mg/Si fractionation in the solar nebula and for Si in the Earth's core. *Earth Planet. Sci. Lett.* **2009**, *287*, 77–85.
27. Fischer, R.A.; Campbell, A.J. The axial ration of hcp Fe and Fe-Ni-Si alloys to the conditions of Earth's nner core. *Am. Mineral.* **2015**, *100*, 2718–2724.
28. Morard, G.; Andrault, D.; Guignot, N.; Siebert, J.; Garbarino, G.; Antonangeli, D. Melting of Fe-Ni-Si and Fe-Ni-S alloys at magabar pressure: Implications for the core-mantle boundary temperature. *Phys. Chem. Miner.* **2011**, *38*, 767–776.
29. Dorogokupets, P.I.; Dewaele, A. Equation of state of MgO, Au, Pt, NaCl-B1 and NaCl-B2: Internally consistent high-temperature pressure scale. *High Press. Res.* **2012**, *27*, 431–446.
30. Dewaele, A.; Belonoshko, A.B.; Garbarino, G.; Occelli, F.; Bouvier, P.; Hanfland, M.; Mezouar, M. High-pressure high-temperature equation of state of KCl and KBr. *Phys. Rev. B* **2012**, *85*, 214105.
31. Campbell, A.J.; Danielson, L.; Righter, K.; Seagle, C.T.; Wang, Y.; Prakapenka, V.B. High pressure effects on the iron-iron oxide and nickel-nickel oxide oxygen fugacity buffers. *Earth Planet. Sci. Lett.* **2009**, *286*, 556–564.
32. Prescher, C.; Prakapenka, V.B. DIOPTAS: A program for reduction of two-dimensional X-ray diffraction data and data exploration. *High Press. Res.* **2015**, *35*, 223–230.
33. Petříček, V.; Dusek, M.; Palatinus, L. Crystallographic computing system JANA2006: General features. *Z. Krist. Cryst. Mater.* **2014**, *229*, 345–352.
34. Angel, R.J.; Equation of state. High-temperature and high-pressure crystal chemistry. *Rev. Mineral. Gepchemistry* **2000**, *41*, 445–520.

35. Klotz, S.; Chervin, J.C.; Munsch, P.; Le Marchand, G. Hydrostatic limit of 11 pressure transmitting media. *J. Phys. D Appl. Phys.* **2009**, *42*, 075413.
36. Dewaele, A.; Loubeyre, P.; Mezouar, M. Equation of state of six metals above 94 GPa. *Phys. Rev. B* **2004**, *70*, 094112.
37. Dewaele, A.; Torrent, M.; Loubeyre, P.; Mezouar, M. Compression curves of transition metals in the Mbar range: Experiments and projector augmented-wave calculations. *Phys. Rev. B* **2008**, *78*, 104102.
38. Dorfman, S.M.; Prakapenka, V.B.; Meng, Y.; Duffy, T.S. Intercomparison of pressure standards (Au, Pt, Mo, MgO, NaCl and Ne) to 2.5 Mbar. *J. Geophys. Res.* **2012**, *117*, B08210.
39. Ye, Y.; Prakapenka, V.B.; Meng, Y.; Shim, S.-H. Intercomparison of the gold, platinum and MgO pressure scales up to 140 GPa and 2500 K. *J. Geophys. Res. Solid Earth* **2017**, *122*, 3450–3464.
40. Dewaele, A.; Loubeyre, P. Pressurizing conditions in helium-pressure-transmitting-medium. *High Press. Res.* **2007**, *27*, 419–429.
41. Bina, C.R.; Hellfrich, G.R. Calculation of Elastic Properties from Thermodynamic Equation of State Principles. *Annu. Rev. Earth Sci.* **1992**, *20*, 527–552.
42. Fischer, R.A.; Campbell, A.J.; Caracas, R.; Reaman, D.M.; Dera, P.; Prakapenka, V.B. Equation of state and phase diagram of Fe-16Si alloy as a candidate component of Earth's core. *Earth Planet. Sci. Lett.* **2012**, *357–358*, 268–276.
43. Fischer, R.A.; Campbell, A.J.; Caracas, R.; Reaman, D.M.; Heinz, D.L.; Dera, P.; Prakapenka, V.B. Equation of state in the Fe-FeSi system at high pressures and temperatures. *J. Geophys. Res. Solid Earth* **2014**, *119*, 2810–2827.
44. Attanayake, J.; Cormier, V.F.; De Silva, S.M. Uppermost inner core seismic structure—New insights from body waveform inversion. *Earth Planet. Sci. Lett.* **2014**, *385*, 49–58.
45. Deuss, A. Heterogeneity and anisotropy of Earth's inner core. *Annu. Rev. Earth Planet. Sci.* **2014**, *42*, 103–126.
46. Lythgoe, K.H.; Deuss, A.; Rudge, J.F.; Neufeld, J.A. Earth's inner core: Innermost inner core or hemispherical variations? *Earth Planet. Sci. Lett.* **2014**, *385*, 181–189.
47. Antonangeli, D.; Merkel, S.; Farber, D.L. Elastic anisotropy of in hcp metals at high pressure and the sound wave anisotropy of the Earth's inner core. *Geophys. Res. Lett.* **2006**, *33*, L24303.
48. Lincot, A.; Cardin, P.; Deguen, R.; Merkel, S. Multiscale model of global inner-core anisotropy induced by hcp alloy plasticity. *Geophys. Res. Lett.* **2016**, *43*, 1084–1091.
49. Gannarelli, C.M.S.; Alfé, D.; Gillan, M.J. The axial ration of hcp iron at the conditions of the Earth's inner core. *Phys. Earth Planet. Inter.* **2005**, *152*, 67–77.
50. Vočadlo, L.; Dobson, D.P.; Wood, I.G. Ab initio calculations of the elasticity of hcp-Fe as a function of temperature at inner-core pressure. *Earth Planet. Sci. Lett.* **2009**, *288*, 534–538.

© 2020 by the authors. Licensee MDPI, Basel, Switzerland. This article is an open access article distributed under the terms and conditions of the Creative Commons Attribution (CC BY) license (http://creativecommons.org/licenses/by/4.0/).